

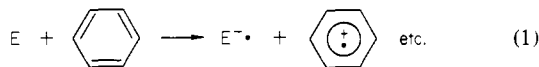
Kinetics and Mechanism of Aromatic Oxidative Substitutions via Electron Transfer. Application of Marcus Theory to Organic Processes in the Endergonic Region

C. J. Schlesener, C. Amatore, and J. K. Kochi*

Contribution from the Department of Chemistry, Indiana University, Bloomington, Indiana 47405. Received September 15, 1983

Abstract: Oxidative substitution of methylarenes by iron(III) complexes proceeds via initial electron transfer to afford benzylic products in excellent yields. The growth and decay of the cation radical ArCH_3^+ (as the prime transient intermediate) are observed directly by its ESR spectrum. The stoichiometric requirement of two Fe(III) is established for various methylarenes ArCH_3 . The rate-limiting electron-transfer process $[\text{ArCH}_3 + \text{Fe(III)} \xrightarrow{k_1} \text{ArCH}_3^+ + \text{Fe(II)}]$ can be excised from the complex kinetics by systematically studying the dependence on added Brønsted bases, which rapidly deprotonate ArCH_3^+ . The validity of the kinetic technique to yield rate constants k_1 for electron transfer, k_{-1} for back electron transfer, and k_3 for subsequent deprotonation is demonstrated for a general mechanism consisting of a fast equilibrium (redox) and a follow-up step (proton transfer). The driving force for electron transfer can be accurately and unambiguously determined in this system by independent measurements of the standard oxidation potentials, i.e., E_{Ar}° for the methylarenes and E_{Fe}° for the iron(II) complexes. The experimental free energy relationship between the rates ($\ln k_1$) of electron transfer and the driving forces $\Delta G_0 = [F(E_{\text{Ar}}^\circ - E_{\text{Fe}}^\circ)]$ can thus be established for the first time in an organic system. There is excellent agreement with the theoretical free energy relationship developed by Marcus for outer-sphere electron transfer. Marcus theory enables the intrinsic barrier for electron transfer from arenes to be quantitatively described in terms of solvation and Jahn-Teller distortion of arene cation radicals. Since electron transfer from methylarenes to iron(III) complexes occurs in the endergonic region of the driving force, the diffusional contribution to the rate constant k_1 must be explicitly taken into account. Procedures are described for the quantitative evaluation of diffusion in terms of either the driving force (normalized to the intrinsic barrier) or the Brønsted slope, and the relevance to organic systems generally is presented.

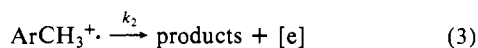
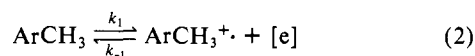
Aromatic substitution remains one of the most fundamental transformations in organic chemistry. By far the most common mechanism involves direct electrophilic attack on the aromatic nucleus to form the Wheland (σ -complex) intermediate.¹ However, many electrophiles are also known to be electron acceptors (i.e., oxidants).² Thus it is not always easy to make an unequivocal mechanistic distinction between such a concerted activation process and one involving prior electron transfer.³ Indeed there are many examples of aromatic compounds undergoing one-electron oxidation by a variety of electron acceptors E, particularly the metal-centered ones such as Tl(III), Hg(II),



Pb(IV), Co(III), Pd(II), Fe(III), Ce(IV), Mn(III), Ag(II), etc.⁴ Since some of these acceptors also participate in aromatic substitution,⁵ the redox system offers an opportunity to evaluate the relevance of electron transfer to aromatic donors. Previous studies of arene oxidation have been mainly directed toward product identification and stoichiometry.⁶ Although there are a few kinetic studies,^{7,8} there are none in which the rate-limiting step in eq 1 has been unambiguously identified and the rate of electron transfer measured.⁹ The absence of such definitive studies is understandable if one considers the general kinetics problem of coping with reversibility (i.e., the competing rate of back electron transfer), especially when the driving force for eq 1 is endergonic.¹⁰

In order to establish the mechanism of electron transfer from aromatic compounds, we chose the oxidation of various methylarenes by a series of tris(phenanthroline)iron(III) complexes which are constrained to effect single electron transfer.^{11,12} Moreover, methylarenes ArCH_3 are useful aromatic donors for these kinetic studies since they are known to undergo substitution via the arene cation radical formed by either electrochemical or chemical oxidation.^{4,13} The kinetic scheme outlined by eq 2 and 3 is a classical

Scheme I



example of an ECE process commonly encountered in the electrochemical literature.¹⁴⁻¹⁸ (Note [e] represents the reduced oxidant or electrode.) As such, the general problem reduces to the determination of the rate constant k_1 under conditions in which

(1) Lowry, T. H.; Richardson, K. S. "Mechanism and Theory in Organic Chemistry", 2nd ed.; Harper and Row: New York, 1981.

(2) See, e.g.: Fukuzumi, S.; Kochi, J. K. *J. Org. Chem.* **1981**, *46*, 4116.

(3) (a) Perrin, C. L. *J. Am. Chem. Soc.* **1977**, *99*, 5516. (b) Kochi, J. K. *Tetrahedron Lett.* **1974**, 4305.

(4) Sheldon, R. A.; Kochi, J. K. "Metal Catalyzed Oxidation of Organic Compounds"; Academic Press: New York, 1981.

(5) For example, see: McKillop, A.; Turrell, A. G.; Young, D. W.; Taylor, E. C. *J. Am. Chem. Soc.* **1980**, *102*, 6504 and related papers. See also: Elson, I.; Kochi, J. K. *Ibid.* **1973**, *95*, 5060.

(6) Beletskaya, I. P.; Makhon'kov, D. I. *Russ. Chem. Rev.* **1981**, *50*, 1007.

(7) (a) Andrulis, P. J.; Dewar, M. J. S.; Deitz, R.; Hunt, R. L. *J. Am. Chem. Soc.* **1966**, *88*, 5473. (b) Ebersson, L. *Ibid.* **1983**, *105*, 3192.

(8) (a) Kimura, M.; Yamabe, S.; Minato, T. *Bull. Chem. Soc. Jpn.* **1981**, *54*, 1699. (b) Bhattacharjee, A. K.; Mahanti, M. K. *Gazz. Chim. Ital.* **1983**, *113*, 1. (c) Baciocchi, E.; Mandolini, L.; Rol, C. *J. Am. Chem. Soc.* **1980**, *102*, 7597.

(9) (a) The results presented in ref 8c were analyzed in terms of Marcus theory by Ebersson^{9b,c} despite the fact that the rate constants reported in ref 8c are representative of a complex kinetic behavior (see, e.g., ref 5 in ref 8c). (b) Ebersson, L. *Adv. Phys. Org. Chem.* **1982**, *18*, 79. (c) See in particular row 13 in Table XVI of ref 9b.

(10) See: Klingler, R. J.; Kochi, J. K. *J. Am. Chem. Soc.* **1982**, *104*, 4186. For highly endergonic reactions, k_{-1} can approach the diffusion-controlled limit of $10^9\text{--}10^{10} \text{ M}^{-1} \text{ s}^{-1}$.

(11) Schilt, A. A. "Analytical Applications of 1,10-Phenanthroline and Related Compounds"; Pergamon: Oxford, 1969.

(12) See, e.g.: (a) Dulz, G.; Sutin, N. *Inorg. Chem.* **1963**, *2*, 917. (b) Diebler, H.; Sutin, N. *J. Phys. Chem.* **1964**, *68*, 174. (c) Wilkins, R. G.; Yelin, R. E. *Inorg. Chem.* **1968**, *7*, 2667. (d) Wong, C. L.; Kochi, J. K. *J. Am. Chem. Soc.* **1979**, *101*, 5593. (e) Fukuzumi, S.; Kochi, J. K. *Ibid.* **1982**, *104*, 7599.

(13) (a) Nyberg, K. In "Encyclopedia of Electrochemistry of the Elements"; Bard, A. J., Lund, H., Eds.; Marcel Dekker: New York, 1978; Vol. XI, Chapter XI-1, "Alkyl Aromatic Compounds", pp 43-70. (b) Ebersson, L.; Nyberg, K. *Acc. Chem. Res.* **1973**, *6*, 106 and references therein.

(14) Baumberger, R. S.; Parker, V. D. *Acta Chem. Scand., Ser. B* **1980**, *B34*, 537.

(15) Amatore, C.; Saveant, J. M. *J. Electroanal. Chem.* **1983**, *144*, 59. (16) Aalstad, B.; Ronlan, A.; Parker, V. D. *Acta Chem. Scand., Ser. B* **1981**, *B35*, 649.

(17) (a) Bewick, A.; Edwards, G. J.; Mellor, J. M.; Pons, B. S. *J. Chem. Soc., Perkin Trans. 2* **1977**, 1952. (b) Bewick, A.; Mellor, J. M.; Pons, B. S. *Electrochim. Acta* **1980**, *25*, 931.

(18) Amatore, C.; Saveant, J. M. *J. Electroanal. Chem.* **1977**, *85*, 27; **1979**, *102*, 21; **1981**, *123*, 189.

* Present address: Department of Chemistry, University of Houston, University Park, Houston, Texas 77004.

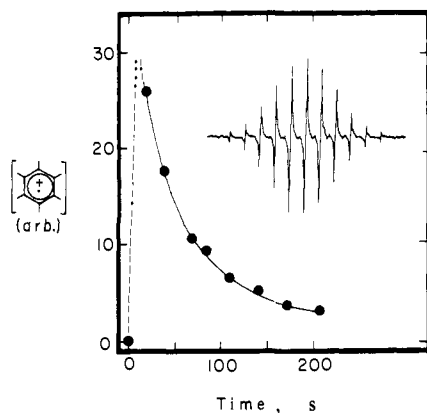
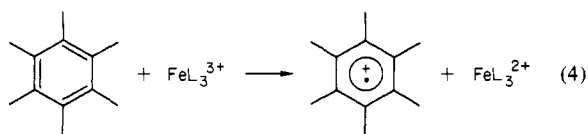


Figure 1. Growth and decay of the cation radical derived from the oxidation of 3×10^{-3} M hexamethylbenzene by $\sim 1 \times 10^{-3}$ M tris(phenanthroline)iron(III) in trifluoroacetic acid at 25 °C. The well-resolved ESR spectrum of HMB^+ taken during the reaction (-31 °C) is shown in the inset.

the fast equilibrium in eq 2 is displaced by the follow-up step(s) in eq 3. Thus our first objective in this study is to develop a kinetic system for the measurement of the rate constant k_1 for electron transfer and then to evaluate the structural effects of aromatic donors on the activation process for electron transfer within the context of the Marcus rate theory.¹⁹

Results and Discussion

When a solution of tris(phenanthroline)iron(III) (FeL_3^{3+}) is mixed with an arene such as hexamethylbenzene HMB in either acetonitrile or trifluoroacetic acid, there is a color change from blue to red indicative of the reduction of the iron(III) complex to iron(II). The formation of a transient intermediate is demonstrated in Figure 1 by the growth and decay of the ESR signal of the arene cation radical,²⁰ i.e.,



I. Products and Stoichiometry. Methylarenes upon oxidation are known to produce both side-chain and nuclear substitution products when carried out either electrochemically or chemically.^{6,13} For example, the permethylated hexamethylbenzene affords excellent yields of pentamethylbenzyl acetate and trifluoroacetate when these oxidations are carried out in acetic and trifluoroacetic acids, respectively.²¹ Moreover, the corresponding *N*-benzylacetamide can be isolated in high yields when the medium is acetonitrile contaminated with adventitious water.²² In anhydrous acetonitrile containing small amounts of added pyridine, the predominant oxidation product is the *N*-benzylpyridinium salt (see Experimental Section). It is reasonable to expect that all of these products of side-chain substitution share the corresponding benzyl cation²³ as a common precursor, i.e.,



since even weak bases that are structurally diverse as CF_3CO_2^- , CH_3CN ,¹⁷ py, etc., can serve effectively as X in eq 5.

In the presence of a slight excess of arene, the iron(III) oxidant is reduced completely to the iron(II) species, tris(phenanthroline)iron(II), as verified by examination of the characteristic visible absorption spectrum.¹¹ Spectral titration of the iron species by

(19) (a) Marcus, R. A. *J. Chem. Phys.* **1956**, *24*, 4966; (b) *Ibid.* **1965**, *43*, 679.

(20) Cf.: Dessau, R. M.; Shih, S.; Heiba, E. I. *J. Am. Chem. Soc.* **1970**, *92*, 412.

(21) Ebersson, L.; Nyberg, K. *J. Am. Chem. Soc.* **1966**, *88*, 1686. Svanholm, U.; Parker, V. D. *Tetrahedron Lett.* **1972**, 471. See also the Experimental Section of this paper.

(22) Ebersson, L.; Nyberg, K. *Tetrahedron Lett.* **1966**, 2389. See also the Experimental Section of this paper.

(23) Rollick, K. L.; Kochi, J. K. *J. Am. Chem. Soc.* **1982**, *104*, 1319.

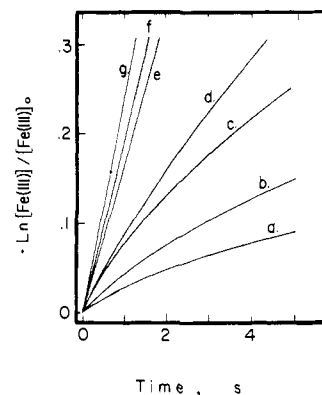


Figure 2. Effect of pyridine on the rate of disappearance of 1.2×10^{-4} M $\text{Fe}(\text{phen})_3^{3+}$ during the oxidation of 3.31×10^{-3} M HNB in acetonitrile at 22 °C. Added pyridine: (a) 0, (b) 0.4, (c) 1.0, (d) 5.0, (e) 50, (f) 500, (g) 5000 equiv relative to iron(III).

the method of continuous variations²⁴ indicated that 2 mol of iron(III) were reduced for each mole of arene oxidized, as described in the Experimental Section. In order to carry out an additional check of this stoichiometry, the consumption of arene was measured by quantitative gas chromatography and related directly to the amount of iron(II) produced. Accordingly, the stoichiometry of the side-chain oxidative substitution of the methylarenes pertinent to this study can be described by the general relationship:²⁵

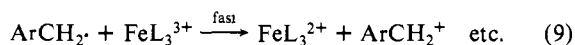


where $[\text{X}] = \text{CF}_3\text{CO}_2^-, \text{CH}_3\text{CN}$,²⁶ py, etc.

II. Kinetics of Arene Oxidative Substitution. The Effect of Bases. The kinetics of the oxidative substitution were followed at 22 °C by measuring the disappearance of the iron(III) complex spectrally at 650 nm ($\epsilon 540 \text{ M}^{-1} \text{ cm}^{-1}$) in acetonitrile. The same results were obtained by following the appearance of iron(II) product at 510 nm ($\epsilon 1.1 \times 10^4 \text{ M}^{-1} \text{ cm}^{-1}$). In the presence of excess arene (HMB to approximate zero-order kinetic conditions), the rate of disappearance of iron(III) does not follow pseudo-first-order kinetics, as shown by curve a in Figure 2. However, we noted that the addition of Brønsted bases had a marked effect on the rate. For example, Figure 2 illustrates that as little as 0.4 equiv of pyridine has a noticeable kinetic effect (curve b), and 1 equiv of pyridine is sufficient to increase the rate by >3-fold (curve c). (Control experiments in the absence of arene established that the reduction of iron(III) by pyridine itself was much too slow to account for the rate enhancement.) Examination of the results in Figure 2 also shows that the rate followed an increasingly first-order (i.e., linear) dependence on iron(III) as the concentration of pyridine was increased. At ~ 5000 equiv of pyridine, the kinetics were essentially first order (to within 10%) for at least one half-life, as shown in curve g, Figure 2.

In order to extract the rate constant for electron transfer from these experiments, let us consider the mechanism for iron(III) reduction that derives from the ECE process outlined in Scheme I above, i.e.,

Scheme II



(24) Rossotti, F. J. C.; Rossotti, H. "Determination of Stability Constants"; McGraw-Hill: New York, 1961; p 47.

(25) Products of nuclear substitution $\text{X}-\text{ArCH}_3$ are formed in minor amounts with the same stoichiometry.

(26) As the acetamido derivative after hydrolysis.^{17,22}

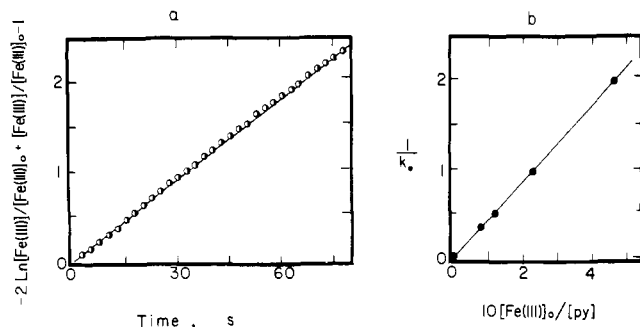


Figure 3. (a) Kinetics of the oxidation of *p*-methoxytoluene by $\text{Fe}(\text{phen})_3^{3+}$ in acetonitrile according to eq 12. (b) The pseudo-first-order dependence of the experimental rate constant k_e on added pyridine.

It is important to note that Scheme II together with eq 5 account completely for the observed products and stoichiometry of oxidative substitution, as well as the ESR observation in Figure 1 of the arene cation radical as a transient intermediate.

In Scheme II the role of pyridine is to displace the redox equilibrium in eq 7 by proton removal from the arene cation radical in the follow-up reaction (eq 8). (Independent experiments previously established²³ that the oxidation of benzyl radicals by FeL_3^{3+} to afford benzyl cations in eq 9 has a second-order rate constant exceeding $10^6 \text{ M}^{-1} \text{ s}^{-1}$.) Accordingly, the consideration of the steady-state behaviors of $[\text{ArCH}_3^{\cdot+}]$ and $[\text{ArCH}_2^{\cdot}]$ leads to the rate law for the disappearance of iron(III) as:

$$\left\{ 1 + \frac{k_{-1}[\text{Fe(III)}]_0}{k_3[\text{py}]} \right\} \ln \frac{[\text{Fe(III)}]}{[\text{Fe(III)}]_0} + \left\{ \frac{k_{-1}[\text{Fe(III)}]_0}{k_3[\text{py}]} \right\} \left\{ 1 - \frac{[\text{Fe(III)}]}{[\text{Fe(III)}]_0} \right\} = -2k_1[\text{ArCH}_3]_0 t \quad (10)$$

where $[\text{Fe(III)}]_0$ and $[\text{Fe(III)}]$ represent the concentrations of tris(phenanthroline)iron(III) initially and at time t , respectively, and $[\text{ArCH}_3]_0$ is the concentration of methylarene in >10-fold excess (see Experimental Section). The general rate expression in eq 10²⁷ gives rise to two limiting kinetic situations that are determined by the rate of the back electron transfer relative to that of the follow-up reaction and indicated by the magnitude of the ratio²⁸ $k_{-1}[\text{Fe(III)}]_0/(k_3[\text{py}])$.

(a) When $[\text{py}]$ is low and this ratio is large (i.e., electron transfer is equilibrated and proton loss is rate limiting), the rate expression is

$$\ln \frac{[\text{Fe(III)}]}{[\text{Fe(III)}]_0} + 1 - \frac{[\text{Fe(III)}]}{[\text{Fe(III)}]_0} = -2 \frac{k_3 k_1}{k_{-1}} \left\{ \frac{[\text{ArCH}_3]_0 [\text{py}]}{[\text{Fe(III)}]_0} \right\} t \quad (11)$$

At pyridine concentrations sufficient to approximate zero-order conditions, eq 11 can be simply represented as²⁷

$$\ln \frac{[\text{Fe(III)}]}{[\text{Fe(III)}]_0} + 1 - \frac{[\text{Fe(III)}]}{[\text{Fe(III)}]_0} = -2k_e[\text{ArCH}_3]_0 t \quad (12)$$

Indeed this kinetic situation is encountered with arenes such as *p*-methoxytoluene shown in Figure 3a, in which the experimental rate constant k_e is proportional to the pyridine concentration (compare eq 11 and 12 and see Figure 3b).²⁹

(b) At the other extreme when $[\text{py}]$ is high and the ratio $k_{-1}[\text{Fe(III)}]_0/(k_3[\text{py}])$ is small (i.e., electron transfer is slow

Table I. Standard Oxidation Potentials of Various (Phenanthroline)iron(II) Complexes and Methylarenes^a

$(\text{X}(\text{phen}))_3 \text{I}^+ \text{e}^{2+}$ X	$E_{\text{Fe}^{\circ}}$, V vs. SCE	methylarene	$E_{\text{Ar}^{\circ}}$, V vs. SCE
H	1.09		1.62
5-Cl	1.19		1.75
5-NO ₂	1.29		1.83
			1.82

^a In either acetonitrile or from data in trifluoroacetic acid, as described in the Experimental Section.

relative to proton loss), the general rate law in eq 10 simplifies to

$$\ln \frac{[\text{Fe(III)}]}{[\text{Fe(III)}]_0} \approx -2 \left\{ \frac{k_1}{1 + (k_{-1}[\text{Fe(III)}]_0/k_3[\text{py}])} \right\} [\text{ArCH}_3]_0 t \quad (13)$$

$$= -2k_e'[\text{ArCH}_3]_0 t \quad (14)$$

Thus at this extreme the kinetics are expected to approximate pseudo-first-order behavior which leads to an experimental rate constant k_e' dependent on the pyridine concentration.³⁰ Indeed both expectations accord with the experimental results shown in Figure 2 for those oxidation runs in curves e, f, and g for which $[\text{py}] = 50, 500, \text{ and } 5000 \text{ equiv}$, respectively.³¹

III. Determination of the Electron-Transfer Rate Constants k_1 and k_{-1} and the Deprotonation Rate Constant k_3 . Deuterium Kinetic Isotope Effects. The foregoing analysis indicates that oxidative substitutions carried out at suitably high base concentrations are primarily limited by the rate of electron transfer. As such, the experimental rate constant k_e' for electron transfer can be expressed by the combination of eq 13 and 14 as

$$\frac{1}{k_e'} = \frac{1}{k_1} + \frac{k_{-1}}{k_1 k_3} \frac{[\text{Fe(III)}]_0}{[\text{py}]} \quad (15)$$

The experimental dependence of this rate constant on the base concentration is illustrated in Figure 4 for various methylarenes and pyridine bases. In each of these plots, the intercept yields the intrinsic rate constant k_1 for electron transfer directly.

According to eq 15, the slope of the plots in Figure 4 represents the ratio of rate constants $k_{-1}/(k_1 k_3)$. Since k_1/k_{-1} is the equilibrium constant for the electron exchange in eq 7, it is related to the overall free energy change ΔG_0 and can be expressed as³²

$$\frac{k_1}{k_{-1}} = \exp(-\Delta G_0/RT) = \exp[\mathcal{F}(E_{\text{Fe}^{\circ}} - E_{\text{Ar}^{\circ}})/(RT)] \quad (16)$$

where $E_{\text{Fe}^{\circ}}$ and $E_{\text{Ar}^{\circ}}$ are the standard oxidation potentials of FeL_3^{2+} and ArCH_3 , respectively, and \mathcal{F} is the Faraday constant. Both of these standard potentials were measured by cyclic volt-

(27) A similar rate expression was obtained by Ebersson for the oxidation of *p*-methoxytoluene by $\text{Co}^{\text{III}}\text{W}_{12}\text{O}_{40}^{5-}$ in aqueous acetic acid with acetate as a base.^{7b}

(28) The back electron transfer is actually given by $2xk_{-1}[\text{Fe(III)}]_0$ where $2x$ is the extent of reaction (i.e., $[\text{Fe(II)}]/[\text{Fe(III)}]_0$) and constant at a given time.

(29) The full kinetics of this system will be elaborated later. Note in Figure 3b, $1/k_e$ is plotted vs. $1/[\text{py}]$ for a better comparison with the systems in Figure 4.

(30) Pseudo-first-order kinetics are of course only reached at the limit of $k_{-1}[\text{Fe(III)}]_0/(k_3[\text{py}]) = 0$. Considering the experimental uncertainties, however, this situation is met as soon as the ratio is less than 0.5, as elaborated in the Experimental Section.

(31) Similar effects were observed with the sterically hindered 2,6-lutidine (vide infra). The use of structurally different bases such as CsF, Bu_4NCl , LiO_2CCF_3 , Bu_4NOH , and water were restricted owing to their competing reactions with FeL_3^{3+} in acetonitrile.

(32) Bard, A. J.; Faulkner, L. R. "Electrochemical Methods"; Wiley: New York, 1980.

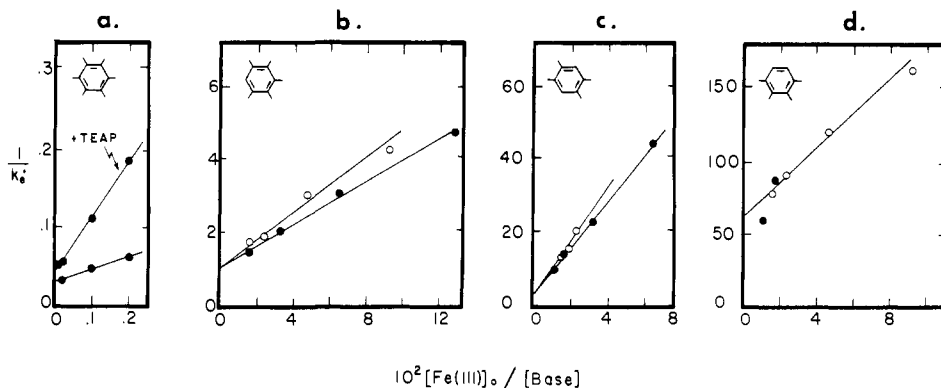


Figure 4. Dependence of the experimental rate constant k_e' for the oxidative substitution of (a) hexamethylbenzene, (b) pentamethylbenzene, (c) durene, and (d) prehnitene by $\text{Fe}(\text{phen})_3^{3+}$ on the concentration of pyridine (●) and 2,6-lutidine (○), added as bases. The effect of 0.1 M tetramethylammonium perchlorate is shown in a.

Table II. Determination of Second-Order Rate Constants for Electron Transfer and Deprotonation^a

methylarene	$(5\text{-X}(\text{phen}))_3\text{Fe}^{3+}$ X	k_1	k_{-1}	k_3	
				py	lu ^c
 HMB	H	14 (38) ^b	1.3×10^8	1.5×10^5 ^d	
	Cl	52 ^e	9.5×10^6		
	NO ₂	1300 ^e	4.8×10^6		
 PMB	H	15	1.4×10^8	5.5×10^4	
	H	0.28	4.1×10^8		
 DUR	Cl	5.3 ^e	1.6×10^8	4.0×10^6	
	NO ₂	75 ^e	4.4×10^7		
	H	3.0×10^{-2}	1.0×10^9		
 TMB	Cl	3.8	2.6×10^9	2.2×10^7	
	NO ₂	16	2.2×10^8		
	H	5.1×10^{-3}	1.2×10^8		
	Cl	2.8	1.3×10^9		
	NO ₂	4.1	3.7×10^7		

^a In acetonitrile maintained at 22 °C and at constant ionic strength with 0.1 M TEAP and containing excess methylarene, unless otherwise stated. Second-order rate constants in $\text{M}^{-1} \text{s}^{-1}$. ^b Determined in the absence of 0.1 M TEAP, unless indicated otherwise. ^c 2,6-Lutidine. ^d Value of $k_3 = 7.1 \times 10^5$ obtained in the absence of added TEAP. ^e Kinetic studies carried out under second-order conditions. See Experimental Section for concentrations employed.

ammetric techniques as described in the Experimental Section, and their values are summarized in Table I.

The independent determination of k_1/k_{-1} thus allows the rate constant k_3 for deprotonation of the cation-radical ArCH_3^+ to be evaluated from the slopes in Figure 4. The separate values of k_1 , k_{-1} , and k_3 obtained in this manner are listed in Table II for systems consisting of various methylarenes and substituted (phenanthroline)iron(III) oxidants in the presence of several pyridine bases. Since the intrinsic rate constant k_1 listed for the first entry in Table II was subject to a small negative salt effect, all kinetic measurements were carried out at constant ionic strength with 0.1 M tetraethylammonium perchlorate (TEAP). In the same system, the deprotonation rate constant k_3 was subject to a rather sizable negative salt effect, decreasing from $7.1 \times 10^5 \text{ M}^{-1} \text{ s}^{-1}$ in the absence of added salt to $1.5 \times 10^5 \text{ M}^{-1} \text{ s}^{-1}$ in the presence of 0.1 M TEAP (see Figure 4a).³³

The kinetic isotope effect was examined by comparing the reaction rates of HMB and HMB-*d*₁₈ with those of tris(phenanthroline)iron(III) in the presence of pyridine. The effect of

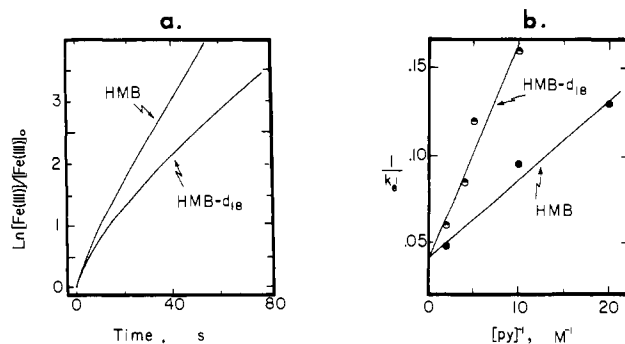
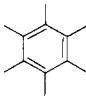
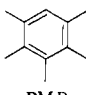
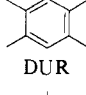
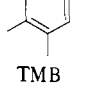
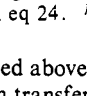


Figure 5. Kinetic effect of deuterium substitution on (a) the rate of oxidation of HMB by $\text{Fe}(\text{phen})_3^{3+}$ and (b) the pyridine dependence of the rate constant k_e' .

deuterium substitution shows up in two ways: (i) on the diminished rate of iron(III) reduction and an increased curvature in Figure 5a, (ii) on the increased slope in Figure 5b, which describes the pyridine dependence of the experimental rate constant according to eq 15. Importantly, the treatment of the data in the manner

(33) The detailed kinetics of ArCH_3^+ deprotonation will be reported separately.

Table III. Free Energy Change, Activation Free Energy, and Intrinsic Barrier for Electron Transfer from Arenes^a

(5-X(phen)) ₃ Fe ³⁺ X	$\Delta G_0'$ b	ΔG^\ddagger c	ΔG_0^\ddagger			$(\Delta G_0^\ddagger)_{av}^h$			
			M ^d	MLA ^e	RW ^f	M ^d	MLA ^e	RW ^f	
	H	11.2	13.4	6.61	6.13	5.43	7.1	6.8	6.3
	Cl	8.86	12.6	7.52	7.26	6.86			
	NO ₂	6.55	10.7	7.04	6.90	6.66			
	H	14.2	15.6	6.59	5.79	4.67	6.6	6.1	5.3
	Cl	11.9	13.9	6.61	6.07	5.27			
	NO ₂	9.55	12.4	6.78	6.45	5.95			
PMB 	H	16.0	16.8	6.23	5.12	3.67	6.3	5.5	4.4
	Cl	13.7	13.4	g	g	g			
	NO ₂	11.4	13.3	6.31	5.79	5.03			
DUR 	H	15.8	18.0	8.20	7.41	6.29	6.8	6.1	5.1
	Cl	13.5	14.0	4.95	3.93	2.65			
	NO ₂	11.2	14.0	7.33	6.90	6.26			
TMB 	H	15.8	18.0	8.20	7.41	6.29	6.8	6.1	5.1
	Cl	13.5	14.0	4.95	3.93	2.65			
	NO ₂	11.2	14.0	7.33	6.90	6.26			

^a Energies in kcal mol⁻¹. ^b Experimental uncertainty is ± 0.5 . ^c Experimental uncertainty is ± 0.1 . ^d Marcus eq 22. ^e Marcus-Levine-Agmon eq 24. ^f Rehm-Weller eq 23. ^g ΔG_0^\ddagger was not evaluated since $\Delta G_0' > \Delta G^\ddagger$. ^h Average value for each arene.

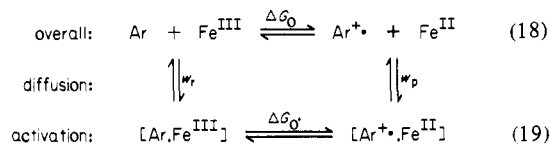
described above yields values of the intrinsic rate constant k_1 for electron transfer that are essentially the same for both HMB and HMB-*d*₁₈ (see the first and fourth entries in Table II). The deuterium kinetic isotope effect of $k_H/k_D = 2.7$ is clearly associated with the deprotonation step. It is gratifying that both results are in accord with the mechanism in Scheme II, since only a small secondary isotope effect is expected for electron transfer,³⁴ and proton loss from the methylarene cation radical should exhibit a primary kinetic isotope effect.³⁵

IV. Free Energy Relationship for Electron-Transfer Rates from Methylarenes. The oxidative substitution of arenes offers a unique opportunity to examine the quantitative relationship between the rate and the driving force for electron transfer, since it is one of the few organic systems in which values of both the intrinsic rate constants [k_1 , k_{-1}] and the free energy changes [$\mathcal{F}(E_{Ar^\circ} - E_{Fe^\circ})$] for electron transfer have been rigorously established. It is noteworthy that the rate constant k_{-1} for back electron transfer listed in Table II falls in the range very close to the diffusion-controlled limit of 10^9 – 10^{10} M⁻¹ s⁻¹.³⁵ As such, neither k_{-1} nor k_1 can be considered to represent only a purely activation process for electron transfer; but they must also include diffusional processes.³⁶ Let us therefore consider the general case in which the measured rate constant k_1 for electron transfer takes into account both contributions, i.e.,

$$\frac{1}{k_1} = \frac{1}{k^*} + \frac{1}{k_r} + \frac{1}{k_p} \exp[\mathcal{F}(E_{Ar^\circ} - E_{Fe^\circ})/(RT)] \quad (17)$$

where k^* represents the true activation rate constant for electron transfer, and k_r and k_p are the diffusion rate constants for the formation of the precursor complex and the successor complex, respectively.^{37,38} Such a formulation derives from the overall

Scheme III



electron transfer in eq 18 considered in terms of the three successive elementary steps outlined below.^{36,37} In Scheme III the diffusion rate constants k_r and k_p refer to the precursor and successor complexes³⁸ (see brackets) in steady state, and the free energy change for the activation process in eq 19 is then given by $\Delta G_0' = \Delta G_0 + (w_p - w_r)$. Since the arene is uncharged, we consider the reactant work term w_r to be nil. Accordingly the free energy change from the precursor to the successor complex in eq 19 is

$$\Delta G_0' = \mathcal{F}(E_{Ar^\circ} - E_{Fe^\circ}) + w_p \quad (20)$$

where w_p is the work term of the ion pair. The computed values (see Experimental Section) of $\Delta G_0'$ are listed in Table III. The free energy of activation ΔG^\ddagger for electron transfer in eq 19 is evaluated from the rate constant by³⁹

$$\Delta G^\ddagger = -RT \ln(k^*/Z) - w_r \quad (21)$$

where the collision frequency Z and the adiabaticity coefficient are taken to be 10^{11} and unity, respectively.^{19,39} The values of ΔG^\ddagger computed with the aid of eq 17 and 21 (see Experimental Section) are also listed in Table III.

(38) We use the designation "precursor or successor complex" to describe the states in which the two molecules are in close contact prior to or after the effective electron transfer. However, we do not imply that these states correspond to energy minima. See ref 36.

(39) As was used here, ΔG^\ddagger refers to the activation free energy for eq 19 and not for the experimentally measured eq 18, for which the activation free energy is $\Delta G^* = (\Delta G^\ddagger + w_r)$ and the rate constant is $k^* = \kappa Z \exp(-\Delta G^*/RT)$.

(40) Equation 22 is applicable in the range of the reorganization energy $\lambda = 4\Delta G_0' \geq |G_0'|$. In the endergonic region for $\lambda > \Delta G_0'$, $\Delta G^\ddagger = \Delta G_0'$. In the exergonic region for $\lambda < \Delta G_0'$, $\Delta G^\ddagger = 0$. See also: Hush, N. S. In "Mechanistic Aspects of Inorganic Reactions", Rorabacher, D. B., Endicott, J. F., Eds.; American Chemical Society: Washington, DC, 1982; ACS Symp. Ser., No. 13, pp 301–329.

(41) Rehm, D.; Weller, A. *Ber. Bunsenges. Phys. Chem.* **1969**, *73*, 834; *Isr. J. Chem.* **1970**, *8*, 259.

(42) Marcus, R. A. *J. Phys. Chem.* **1968**, *72*, 891.

(43) (a) Agmon, N.; Levine, R. D. *Chem. Phys. Lett.* **1977**, *52*, 197. (b) Levine, R. D. *J. Phys. Chem.* **1979**, *83*, 159.

(34) The gas-phase ionization potentials and the standard oxidation potentials of HMB and HMB-*d*₁₈ are the same within experimental uncertainties.

(35) (a) See, e.g.: Moore, J. W.; Pearson, R. G. "Kinetics and Mechanism"; Wiley Interscience: New York, 1981. Cannon, R. D. "Electron Transfer Reactions"; Butterworths: London, 1980. (b) The diffusion limit in acetonitrile is ca. 2×10^{10} M⁻¹ s⁻¹ when one of the particles is uncharged. For k_{-1} , the reaction is between Fe²⁺ and ArH^{•+}. The diffusion controlled rate constant between one particle charged 2+ and one charged 1+, can be evaluated as 3×10^9 M⁻¹ s⁻¹ in acetonitrile from ref 35a and 36.

(36) See, e.g.: Marcus, R. A. *Faraday Discuss. Chem. Soc.* **1960**, *29*, 129. Marcus, R. A.; Siders, P. In "Mechanistic Aspects of Inorganic Reactions"; Rorabacher, D. B., Endicott, J. F., Eds.; American Chemical Society: Washington, DC, 1982; ACS Symp. Ser. No. 10, pp 235–238.

(37) Cf.: Scandola, F.; Balzani, V.; Schuster, G. B. *J. Am. Chem. Soc.* **1981**, *103*, 2519. Andrieux, C. P.; Blocman, C.; Dumas-Bouchiat, J. M.; Saveant, J. M. *J. Am. Chem. Soc.* **1979**, *101*, 3431.

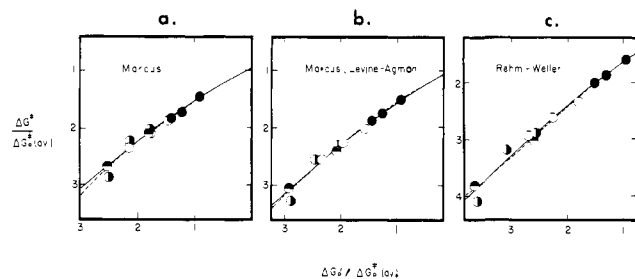


Figure 6. Fit of the measured rate constants k_1 for HMB (●), PMB (○), DUR (◐), and TMB (◑) to the curves representing the free energy relationships by (a) Marcus in eq 22, (c) Rehm-Weller in eq 23, and (b) Marcus-Levine-Agmon in eq 24 and plotted as the activation free energy ΔG^\ddagger against the driving force $\Delta G_0'$, both normalized to the intrinsic barrier ΔG_0^\ddagger . See text for the significance of the dashed lines.

Three different relationships are currently in use to relate the activation free energy ΔG^\ddagger to the free energy change $\Delta G_0'$ in electron-transfer reactions.⁴⁴

$$\text{Marcus:}^{19,40} \quad \Delta G^\ddagger = \Delta G_0^\ddagger \left[1 + \frac{\Delta G_0'}{4\Delta G_0^\ddagger} \right]^2 \quad (22)$$

$$\text{Rehm-Weller:}^{41} \quad \Delta G^\ddagger = \frac{\Delta G_0'}{2} + \left[\left(\frac{\Delta G_0'}{2} \right)^2 + (\Delta G_0^\ddagger)^2 \right]^{1/2} \quad (23)$$

Marcus-Levine-Agmon:^{42,43}

$$\Delta G^\ddagger = \Delta G_0' + \frac{\Delta G_0^\ddagger}{\ln 2} \ln \left\{ 1 + \exp \left[-\frac{\Delta G_0' \ln 2}{\Delta G_0^\ddagger} \right] \right\} \quad (24)$$

All of these free energy relationships employ the intrinsic barrier ΔG_0^\ddagger as the disposable parameter. (The intrinsic barrier represents the activation free energy for electron transfer when the driving force is zero, i.e., $\Delta G^\ddagger = \Delta G_0^\ddagger$ at $\Delta G_0' = 0$.) The last three columns in Table III list the averaged values of the intrinsic barriers for electron transfer for each arene, computed from each of these free energy relationships.⁴⁵ Since the electron exchange in the tris(phenanthroline)iron(III,II) redox couple is known to be very rapid,⁴⁶ the variations of ΔG_0^\ddagger in Table III largely reflect the changes associated with the conversion of the arene to its cation radical. Indeed for a given arene, the value of ΔG_0^\ddagger is found to be relatively invariant with the nature of the iron(III) oxidant. The experimental results thus confirm the validity of eq 22–24 to describe the free energy relationship for electron transfer. This conclusion is graphically illustrated in Figure 6 by the fit of the points to the predicted relationships (see the full curves). (Note the free energy plots are normalized to the intrinsic barrier ΔG_0^\ddagger for each arene, as given by the last three columns in Table III.)

It may be somewhat surprising that no experimental discrimination is possible among eq 22–24, despite their different mathematical forms, each of which appears at first glance to be unique. However, the graphical forms of these free energy relationships are quite similar, as illustrated in Figure 7. Indeed the three curves are coincident in the isergonic region of $\Delta G_0' \approx 0$, and they converge asymptotically to the same endergonic limit

(44) Other models have also been proposed, but apart from differences in their mathematical forms, they appear to be strikingly similar to eq 22–24. Owing to their simplest forms consistent with our data, we will limit ourselves to the classical Marcus model and the Marcus-Levine-Agmon approach. For detailed reviews of various approaches, see, e.g.: (a) Marcus, R. A. *Am. Rev. Phys. Chem.* **1964**, *15*, 155. (b) Schmidt, P. P. *Electrochemistry* **1975**, *15*, 21–131; **1978**, *6*, 128–225. (c) See also ref 49.

(45) For the computations: (a) The diffusion rate constants k_r and k_b for eq 17 were taken to be 2×10^{10} and $3 \times 10^9 \text{ M}^{-1} \text{ s}^{-1}$, respectively.^{35,36} (b) The work term $w_e \approx 0$, and $w_p \approx 1.7 \text{ kcal mol}^{-1}$, was obtained from an electrostatic model of ArCH_3^{2+} and FeL_3^{2+} at a distance, $d^* = r_{\text{Ar}} + r_{\text{Fe}} = 3.5 + 7.0 = 10.5 \text{ \AA}$.

(46) Brunschwigg, B. S.; Creutz, C.; Macartney, D. H.; Sham, T.-K.; Sutin, N. *Faraday Discuss. Chem. Soc.* **1982**, *74*, 113.

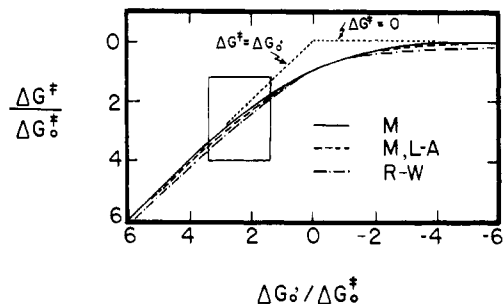


Figure 7. Graphical forms of the free energy relationship according to Marcus (—), Rehm-Weller (---), and Marcus-Levine-Agmon (· · ·), as computed from the free energy values listed in Table III and the averaged values of $\Delta G_0^\ddagger = 6.40, 4.95,$ and $5.80 \text{ kcal mol}^{-1}$, respectively. The diffusion limits are represented by the dotted (· · ·) line. The results of our study pertain to the area enclosed by the rectangle.

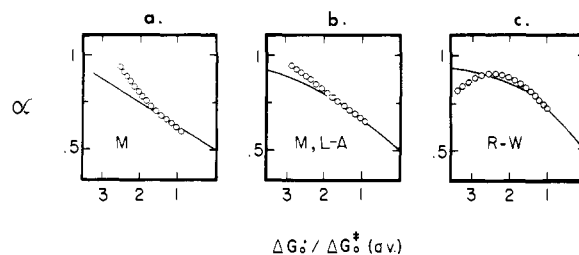


Figure 8. Curves for the variation of the Brønsted slope α as a function of the driving force (normalized to the intrinsic barrier) as calculated from (a) Marcus eq 22, (b) Marcus-Levine-Agmon eq 24, and (c) Rehm-Weller eq 23. The “measured” values of α obtained from the polynomial expansion of the data points are represented by the filled circles.

of $\Delta G^\ddagger = \Delta G_0'$ and to the same exergonic limit of $\Delta G^\ddagger = 0$, in harmony with Hammond's postulate.^{42,47} The largest differences among these predictions do lie in the intermediate regions where $|\Delta G_0^\ddagger| \approx 1/3|\Delta G_0'|$ (see Figure 7). Since our study was also carried out in this transition region, we might inquire whether our data is sufficient to make such a distinction on the basis of either (i) the magnitude of ΔG_0^\ddagger or (ii) the (Brønsted) slope α of the free energy relationship.

(i) A close inspection of the values tabulated in Table III shows no consistent trend in ΔG_0^\ddagger of any significance. Moreover an average estimate of ΔG_0^\ddagger (taking into account all the redox systems and the three relationships⁴⁸) affords $\Delta G_0^\ddagger = 6.0 \text{ kcal mol}^{-1}$ with a standard deviation of only $0.20 \text{ kcal mol}^{-1}$, which is clearly within the experimental accuracy of the data.

(ii) In order to evaluate the experimental slope α of the free energy relationship, the data points in Figure 6 were fitted to the polynomial expansion in eq 25. The form of this polynomial is

$$\frac{\Delta G^\ddagger}{\Delta G_0^\ddagger} = 1 + \frac{1}{2} \left[\frac{\Delta G_0'}{\Delta G_0^\ddagger} \right] + a \left[\frac{\Delta G_0'}{\Delta G_0^\ddagger} \right]^2 + b \left[\frac{\Delta G_0'}{\Delta G_0^\ddagger} \right]^4 \quad (25)$$

dictated by the boundary conditions that at the isergonic point of $\Delta G_0' = 0$, the activation free energy is $\Delta G^\ddagger = \Delta G_0^\ddagger$ and the slope is $\partial \Delta G^\ddagger / \partial \Delta G_0' = 0.5$, both of which are inherent to the symmetry about this point in each of the three models considered here. The following coefficients were obtained from a polynomial regression analysis⁵⁰ of the data in Table III: For the Marcus

(47) (a) Hammond, G. S. *J. Am. Chem. Soc.* **1955**, *77*, 334. See also ref 1 p 197ff. (b) Marcus, R. *Phys. Chem. Sci. Rep.* **1975**, *1*, 477–504.

(48) (a) Although ΔG_0^\ddagger has no theoretical meaning in the empirical Rehm-Weller expression, theoretical support for it in the general framework of Marcus theory has been provided by Efrima and Bixon⁴⁹ and is therefore included here. (b) Note, however, that the most consistent values for ΔG_0^\ddagger with the different arenes are obtained with the Marcus relationship.

(49) Efrima, S.; Bixon, M. *Chem. Phys. Lett.* **1974**, *25*, 34; *Chem. Phys.* **1976**, *13*, 447.

(50) Bevington, P. R. “Data Reduction and Error Analysis for the Physical Sciences”; McGraw-Hill: New York, 1969; pp 137–137.

equation, $a = 0.0525$ and $b = 0.0026$. For the Marcus–Levine–Agmon relationship in eq 24, we found $a = 0.0799$ and $b = -0.0001$. For the Reim–Weller expression in eq 23, $a = 0.1219$ and $b = -0.0033$. These polynomial expressions, which represent the best fit to the experimental data, are replotted as the dashed lines in Figures 6. The experimental variations of the Brønsted slope α were then calculated from the optimized polynomial⁵¹ and are plotted as the points in Figure 8 in the range of the extant data. The full curves in Figure 8, parts a, b, and c, represent the predictions of the free energy relationships in eq 22, 23, and 24, respectively. All three relationships yield Brønsted slopes in the range of $\alpha \sim 0.8$ for electron transfer from arenes. These relatively large values of α are clearly associated with driving forces in the endergonic region.¹⁰ Inspection of Figure 8 shows that eq 22 and 24 are slightly better than eq 23 in predicting the curvature in the free energy relationship for electron transfer. It is noteworthy that all three relationships are quite effective in predicting the absolute magnitudes of the activation free energy as well as its variation with changes in the driving force for electron transfer. Central to these relationships is their ability to afford reasonably consistent measures of the intrinsic barrier ΔG_0^* for electron transfer.

V. Intrinsic Barrier for Electron Transfer from Arenes. Owing to its theoretical significance, we now wish to interpret the magnitude of the intrinsic barrier ΔG_0^* for electron transfer from arenes within the context of the Marcus rate theory.^{19,42} An important feature of Marcus theory is that it allows the prediction of the intrinsic barrier in terms of the reorganization energy, i.e., $\lambda = 4\Delta G_0^*$. For outer-sphere electron transfer, λ can be regarded simply as the sum of two contributions: $\lambda = \lambda_i + \lambda_o$.

The inner-sphere reorganization energy λ_i includes both reactants and takes into account the variations in their bond lengths, bond angles, and any specific interactions attendant upon electron transfer. Since there are no appreciable differences in the experimental bond lengths and angles in tris(phenanthroline)iron(III,II),⁴⁶ λ_i can be regarded as negligible for the iron moiety. However, it is known that benzene undergoes a geometric change arising from the Jahn–Teller distortion in the cation-radical that is generated upon electron transfer.⁵² An estimate of λ_i for the arenes examined in this study can thus be obtained from the value of the stabilization energy of $C_6H_6^+$ relative to the hypothetical cation radical in the nuclear configuration of benzene. Such a reorganization energy has been reported by Salem to be ~ 2.7 kcal mol⁻¹.⁵³

The outer-sphere reorganization energy λ_o arises mainly from the changes in solvation, and can be evaluated from Marcus theory as

$$\lambda_o = (3.35 \times 10^2) \left[\left(\frac{1}{2r_{Ar}} + \frac{1}{2r_{Fe}} \right) - \frac{1}{d^*} \right] \left[\frac{1}{\eta^2} - \frac{1}{D} \right] \quad (26)$$

where r_{Ar} and r_{Fe} are the radii of the reactants considered as hard spheres, and $d^* \cong (r_{Ar} + r_{Fe})$. The index of refraction η and the static dielectric constant D of the solvent acetonitrile are 1.344 and 37.5, respectively.⁵⁴ Taking $r_{Fe} = 7$ Å for tris(phenanthroline)iron(III) complexes⁵⁵ and $r_{Ar} \cong 3.5$ Å for the benzene derivatives,⁵⁶ we calculate λ_o from eq 26 to be 21 kcal mol⁻¹.

The total reorganization energy obtained as the sum of the inner- and outer-sphere contributions can thus be estimated as 24 kcal mol⁻¹. The resulting predicted value of the intrinsic barrier

(51) For the normalized polynomial, $\alpha = \partial(\Delta G^*/\Delta G_0^*)/\partial(\Delta G_0'/\Delta G_0^*) = 0.5 + 2a(\Delta G_0'/\Delta G_0^*) + 4b(\Delta G_0'/\Delta G_0^*)^3$.

(52) (a) Nakajima, T.; Toyota, A.; Kataoka, M. *J. Am. Chem. Soc.* **1982**, *104*, 5610 and references therein. (b) Iwasaki, M.; Toriyama, K.; Nunome, K. *J. Chem. Soc., Chem. Commun.* **1983**, 320.

(53) Salem, L. "The Molecular Orbital Theory of Conjugated Systems"; W. A. Benjamin: New York, 1966; pp 467–485.

(54) "Handbook of Chemistry and Physics"; Weast, R. C., Ed.; CRC Press: Cleveland, 1975.

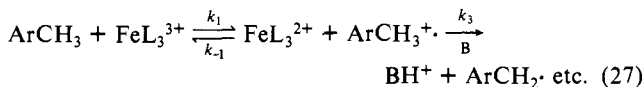
(55) Dickens, J. E.; Basolo, F.; Neumann, H. M. *J. Am. Chem. Soc.* **1957**, *79*, 1289.

(56) Based on an averaged value of r_{Ar} in the plane.

ΔG^* is 6 kcal mol⁻¹, which is in remarkable agreement with the measured value of 6.0 ± 0.2 evaluated from eq 22–24 (vide supra).

Summary and Conclusions

Methylarenes undergo oxidative substitution with 1-equiv oxidants such as tris(phenanthroline)iron(III) according to eq 6. The rate-limiting electron-transfer step to afford the arene cation radical has been successfully extracted from the complex kinetics by carefully analyzing the dependence on the concentration of an added Brønsted base. The base B is responsible for displacement of the redox equilibrium by effecting the deprotonation of the methylarene cation radical in Scheme II (eq 27). The



intrinsic rate constant k_1 for electron transfer, k_{-1} for back electron transfer, and k_3 for deprotonation have all been evaluated for various combinations of methylarenes, substituted (phenanthroline)iron(III) oxidants, and pyridine bases.

The free energy relationship between the rate of electron transfer and the driving force has been rigorously established experimentally. Indeed this system is unique among organic oxidations in that the free energy change ΔG_0 for the metastable redox equilibrium in eq 27 can be quantitatively evaluated directly from independent measurements of the standard oxidation potentials E_{Ar}^0 and E_{Fe}^0 for the various methylarenes and iron(II) complexes, respectively. In order to relate the experimental free energy relationship for electron transfer to the theoretical relationship developed by Marcus,¹⁹ the diffusion rate constants must be explicitly included, as in eq 17. In particular, for endergonic processes of the magnitude encountered in this study, the diffusion rate constant k_p of the product pair can contribute as much as 25% to the measured rate constant k_1 for electron transfer. The same consideration applies to the back electron transfer process, since $k_{-1} = k_1 \exp(\Delta G_0/(RT))$. Therefore let us consider the general description of the rate constant k_1 over the energy gamut (simultaneously covering the endergonic and exergonic limits) in terms of contributions from the activation rate constant k^* and the diffusion rate constant k_d .⁵⁷ Figure 9a shows the variation of k^* with the driving force $\Delta G_0'$ according to Marcus theory (eq 22) for various values of ΔG_0^* . Figure 9b represents the corresponding variations of the diffusion rate constant k_d obtained from eq 17 when $k^* \gg k_r = k_p$,⁵⁷ i.e.,

$$1/k_d = (1/k_r)[1 + \exp(\Delta G_0/(RT))] \quad (28)$$

Figure 9c illustrates how the measured rate constant k_1 (where $1/k_1 = (1/k^*) + (1/k_d)$) varies with the driving force, for various values of ΔG_0^* . To stress the importance of the diffusional contribution to our system, we have represented the k_1 relationship as the heavy line and the corresponding k^* relationship as the dashed line (in each case we employed the average $\Delta G_0^* = 6.7$ kcal mol⁻¹ from our data as deduced from the Marcus equation). The diffusional contribution, represented by the gap between k^* and k_1 , is clearly seen to increase as one proceeds in our system into the endergonic region beyond $\Delta G_0' \sim 7$ kcal mol⁻¹. It is therefore necessary to develop some operational criteria to determine when the diffusional contribution must be explicitly taken into account in the rate process for electron transfer.

Endergonic and exergonic systems (e.g., as applied in the Hammond postulate) are thermodynamic concepts and are of only limited utility in the context of the rate processes of importance here. Let us therefore refer to the endergonic and exergonic *limits*

(57) For the sake of simplicity we assume in the following: $k_r = k_p = k_d$. The rate constant k_d is taken as 5×10^9 M⁻¹ s⁻¹ for an averaged value. See, e.g., ref 35 and: Kojima, H.; Bard, A. J. *J. Am. Chem. Soc.* **1975**, *97*, 6317.

(58) We are actually faced with a conundrum here, since arguments such as those based on the Hammond postulate are most applicable at the endergonic and exergonic limits where the contribution from activation (ΔG^* or ΔH^*) is minor and the rate is controlled by diffusion. Furthermore most kinetic measurements are not carried out at the diffusion limits.

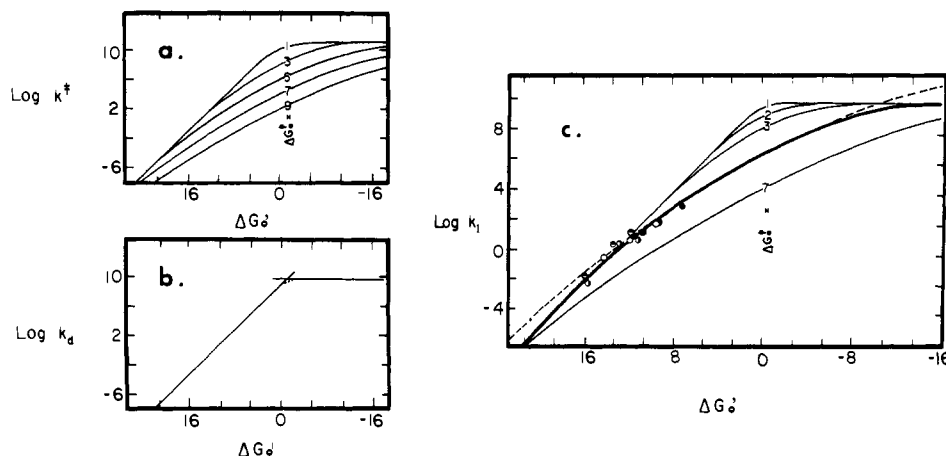


Figure 9. Functional forms of the free energy relationships for the rate constants (a) k^* , (b) k_d , and (c) k_1 : (a) Theoretical curves drawn according to Marcus eq 22 at various values of ΔG_0^* . (b) Hypothetical curve drawn according to eq 28. (c) Curves drawn with various ΔG_0^* according to eq 17 and 22. The heavy solid curve represents the fit to the experimental data for HMB (●), PMB (○), DUR (⊙), and TMB (⊙) with $\Delta G_0^* = 6.7$ kcal mol⁻¹. The dashed line is the free energy relationship drawn according to Marcus eq 22 only, with $\Delta G_0^* = 6.7$ kcal mol⁻¹. (ΔG_0^* is given in units of RT in 10.)

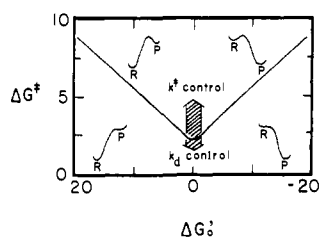


Figure 10. Location of the endergonic and exergonic regions as a function of the intrinsic barrier. The curve is drawn for electron transfer rates arbitrarily chosen to consist of equal activation (k^*) and diffusion (k_d) components. R and P in the reaction diagrams shown in the inset refer to the reactants and products, respectively.

of the kinetics, at which the rates of electron transfer are diffusion controlled. In this context, endergonic and exergonic regions refer to driving forces at which the measured rate constant k_1 contains diffusion components (k_p and k_r) in addition to the activation component (k^*). The driving forces with $|\Delta G_0'| \gg 0$ as the only criterion of endergonicity and exergonicity is inadequate, since the family of curves in Figure 9c clearly shows that the approach of k_1 to the diffusion limits is also strongly dependent on the magnitude of the intrinsic barrier ΔG_0^* for the particular system. For example, the endergonic limit is reached at $\Delta G_0' \cong 5$ kcal mol⁻¹ when $\Delta G_0^* = 2$ kcal mol⁻¹, but the same limit is reached later at 12 kcal mol⁻¹ when ΔG_0^* is doubled. In fact, Figure 10 illustrates how the magnitude of the intrinsic barrier determines the location of the endergonic and exergonic regions. [The curve represents systems with rate constants calculated from eq 17 to consist of (arbitrarily) equal contributions from diffusion and activation. As the systems are displaced above this line, they are increasingly dominated by diffusion.] Since the curve in Figure 10 beyond $|\Delta G_0'| > 1$ kcal mol⁻¹ is reasonably straight, we can conclude that the location of the endergonic and exergonic regions varies more or less linearly with the magnitude of $(\Delta G_0'/\Delta G_0^*)$; i.e., the driving force normalized to the intrinsic barrier. Unfortunately such a criterion is not easy to apply in practice.

Accordingly, let us consider an alternative description of the endergonic and exergonic limits in terms of rate-limiting diffusional processes k_p and k_r with Brønsted slopes of 1 and 0, respectively (see Figure 9b). The endergonic and exergonic regions are then defined as those in which the Brønsted slopes are ~ 1 and ~ 0 , respectively. In order to apply Brønsted slopes as a quantitative criterion, the dependence of the experimental rate constant k_1 (which includes diffusion) in the driving force, i.e., $\partial \ln k_1 / \partial \Delta G_0'$, must be evaluated separately from that involving the activation (theoretical) rate constant k^* . The corresponding values of the experimental and theoretical Brønsted slopes α_1 and α^* , respectively, are plotted as a function of the driving force for arene

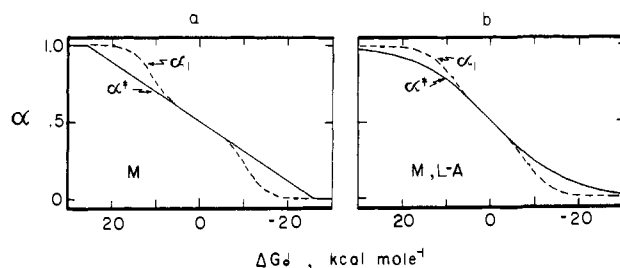


Figure 11. Discrepancy between the measured (α_1) and the theoretical (α^*) Brønsted slopes as a function of the driving force for electron transfer. The values of α_1 were derived from eq 17, and α^* were computed from (a) Marcus eq 22 and (b) Marcus-Levine-Agmon eq 24 with $\Delta G_0^* = 6.7$ and 6.1 kcal mol⁻¹, respectively.

oxidations in Figures 11a,b. [The theoretical Brønsted slopes α^* were computed from both the Marcus eq 22 (Figure 11a) and the Marcus-Levine-Agmon eq 24 (Figure 11b), since each provides a reasonable fit to the experimental data in Figure 8.] The junctions at which the α_1 and α^* curves diverge show that complete activation control of the electron-transfer rates is observed only within a rather narrow window of the driving force, $\Delta G_0' \cong \pm 5$ kcal mol⁻¹, in the endergonic and exergonic regions, respectively. The widening gap beyond this point represents increasing control of the electron-transfer rate by diffusional processes. Since the marked discrepancies between the experimental α_1 and the theoretical α^* characterize the endergonic and exergonic regions, we propose the magnitude of the Brønsted slope to be a useful indicator for rate processes in which diffusion must be explicitly taken into account.

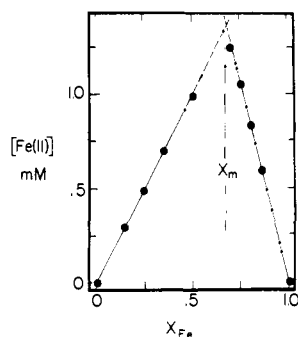
At this juncture, however, we must clearly emphasize that any theoretical argument that relates the magnitude of the Brønsted slope to transition-state structures or diagrams (such as those represented in Figure 10), refers specifically to values of α^* and not α_1 .⁴⁷ Since only α_1 is accessible by experiment, it is important to take explicit cognizance of diffusional contributions when rationalizing the experimental results.⁵⁸ This caveat is particularly pertinent to organic systems in which rates of electron transfer are likely to lie in the endergonic region owing to limiting values of the standard redox potentials and reorganization energies.

Experimental Section

Materials. 1,10-Phenanthroline (Alfa) was recrystallized from toluene prior to use. The substituted phenanthrolines (5-chloro and 5-nitro) were obtained from G. F. Smith Chemical Co. and used as received. The iron(II) complexes were prepared from aqueous ferrous sulfate by the addition of 3 equiv of the appropriate phenanthroline and precipitated with ammonium hexafluorophosphate (Ozark-Mahoning). After collection of $\text{Fe}(\text{phen})_3(\text{PF}_6)_2$ as dark red crystals, they were dried over P_2O_5 in vacuo. The blue iron(III) complex $\text{Fe}(\text{phen})_3(\text{PF}_6)_3$ was prepared by the oxidation of the ferrous complex with ceric ammonium nitrate (G.

Table IV. Extinction Coefficients for the Iron Complexes in Acetonitrile

iron complex	monitor λ , nm (ϵ , M ⁻¹ cm ⁻¹)	ϵ_{550} , M ⁻¹ cm ⁻¹	ϵ_{560} , M ⁻¹ cm ⁻¹
Fe(phen) ₃ (PF ₆) ₂	510 (1.1 × 10 ⁴)	3170	1860
Fe(phen) ₃ (PF ₆) ₃	650 (5.4 × 10 ²)	620	680
Fe(5-Cl(phen)) ₃ (PF ₆) ₃	510 (1.1 × 10 ⁴)		
Fe(5-O ₂ N(phen)) ₃ (PF ₆) ₃	510 (1.4 × 10 ⁴)		

Figure 12. Spectral titration of Fe(phen)₃³⁺ by the method of continuous variation for hexamethylbenzene in acetonitrile.

F. Smith) in aqueous H₂SO₄, followed by precipitation with NH₄PF₆. The substituted phenanthroline complexes of iron(III) were prepared in situ by the electrolytic oxidation of the corresponding iron(II) complexes (vide infra).

Hexamethylbenzene, pentamethylbenzene, and durene (Aldrich) were recrystallized from ethanol, followed by sublimation in vacuo. Prehnitene and *p*-methoxytoluene (Aldrich) were distilled in vacuo prior to use. Hexamethylbenzene-*d*₁₈ (Merck) was kindly donated to us by A. E. Nader (Du Pont). Pyridine and 2,6-lutidine from Matheson, Coleman, and Bell were distilled from KOH pellets before use. Acetonitrile (HPLC grade from Fisher Scientific) was further purified by distillation from CaH₂ through a 15-plate Oldershaw column, followed by stirring overnight with KMnO₄ and Na₂CO₃ (5 g of each per L). The mixture was filtered, distilled under reduced pressure, and finally fractionated from P₂O₅ under an argon atmosphere and stored under argon in a Schlenk flask. Tetraethylammonium perchlorate (G. F. Smith Chemical Co.) was further dried in vacuo.

Stoichiometry of Oxidative Substitution. The stoichiometry was determined by two independent methods involving (A) the spectral titration of the iron(III) oxidant and (B) the consumption of the methylarene as measured by gas chromatography. (A) The method of continuous variations²⁴ was used to monitor the stoichiometry of the reaction of Fe(phen)₃³⁺ with all the arenes. Solutions of 2 × 10⁻³ M Fe(phen)₃³⁺ and 2 × 10⁻³ M methylarene in acetonitrile were mixed in varying ratios while keeping the total volume constant. The mole fraction X_{Fe} of FeL₃³⁺ was varied from 0.15 to 0.85 by using eight samples for each iron(III)-arene pair. In addition, a small amount of base (equimolar to the amount of iron(III) expected to be consumed) was added. The absorbance at 560 nm was recorded (Hewlett-Packard 8450A UV-vis spectrometer) after 24 h, which (with the extinction coefficient of the iron(II,III) complexes in Table IV and the total iron concentration) allowed the concentration of iron(II) to be computed. A typical plot of iron(II) produced against the mole fraction of initial iron(III)₀ is illustrated in Figure 12. The maximum at 0.68 corresponded to X_m = (1 - X_m)S, where the stoichiometry S = [Fe(III)]/[ArCH₃]. (B) The consumption of methylarene was determined directly by the gas chromatographic analysis (20-ft cross-linked methylsilicone capillary column, Hewlett-Packard 5790A/3390A chromatograph/integrator) of the methylarene and the spectral analysis of the iron(II) before and after the addition of iron(III). The separate reactions generally consisted of 0.1 mmol of FeL₃³⁺, 0.05 mmol of ArCH₃, and 0.1 mmol of pyridine in 2 mL of acetonitrile. After 5 days, each solution was treated with a weighed quantity of 1,3,5-tri-*tert*-butylbenzene (serving as the internal standard) and the mixture analyzed by quantitative gas chromatography. The solutions were then treated with diethyl ether to precipitate the iron salts, which were subsequently analyzed spectrally at 550 and 560 nm after dissolution in acetonitrile. Some typical results are presented in Table V for each method.

Products of Oxidative Substitution. Hexamethylbenzene, durene, and *p*-methoxytoluene were selected from among the methylarenes for the quantitative analysis of the substitution products, the authentic samples

Table V. Stoichiometric Consumption of Iron(III) in Aromatic Oxidative Substitutions^a

methylarene	stoichiometry, S = [Fe(III)]/[ArCH ₃]	
	method A	method B
C ₆ (CH ₃) ₆	2.1	1.8
C ₆ H(CH ₃) ₅	2.1	1.8
C ₆ H ₂ (CH ₃) ₄ -1,2,4,5	2.4	3.1 ^b
C ₆ H ₂ (CH ₃) ₄ -1,2,3,4	2.4	2.8 ^b
C ₆ H ₄ (CH ₃)(OCH ₃)-1,2	2.1	1.8

^a In acetonitrile at 25 °C. ^b Subject to error from the competing oxidation of pyridine owing to relatively slow rates of arene consumption.

of which were independently synthesized as follows. The various benzylpyridinium and lutidinium salts were prepared from the corresponding bromides (*p*-CH₃OC₆H₄CH₂Br, 2,4,5-(CH₃)₃C₆H₂CH₂Br)⁵⁹ or chloride ((CH₃)₃C₆H₂CH₂Cl)⁶⁰ with neat pyridine and 2,6-lutidine, respectively. The halide salt was separated from the reaction mixture, washed with ether, and dissolved in water. Addition of excess NH₄PF₆ yielded colorless crystals of the hexafluorophosphate salts, which were readily characterized by their unique singlet resonances at δ ~5.6 for the methylarene protons in the ¹H NMR spectra in acetonitrile (e.g., (CH₃)₃C₆H₂(py)⁺PF₆⁻, δ 5.83; 2,4,5-(CH₃)₃C₆H₂CH₂(lu)⁺PF₆⁻, δ 5.59; *p*-CH₃OC₆H₄CH₂(lu)⁺PF₆⁻, δ 5.73). *N*-(Pentamethylbenzyl)acetamide was prepared by the anodic oxidation of hexamethylbenzene in acetonitrile.²² 2-Methoxy-5-methylacetanilide was prepared by acetylation of the aniline (Aldrich) with acetyl chloride and triethylamine. 2,3,5,6-Tetramethylacetanilide was prepared from the aniline,⁶¹ which was synthesized from durene by bromination⁶² followed by nitration⁶³ and reduction.⁶⁴ The side-chain substitution product *N*-(2,4,5-trimethylbenzyl)acetamide was not independently prepared.²²

The analysis of products resulting from methylarene oxidation was typically carried out as follows. The methylarene (2.4 mmol of *p*-methoxytoluene) and 2,6-lutidine (4.3 mmol) were first dissolved in 2.0 mL of acetonitrile, and then tris(phenanthroline)iron(III) (0.10 mmol) was added. After 1 day, triphenylmethane (0.080 mmol) was added as an internal standard and the ¹H NMR spectrum recorded. The integral of the internal standard at δ 5.5 was compared to that of the benzylic protons of the product at δ 5.7. A similar procedure was used in the conversion of hexamethylbenzene to the (pentamethylbenzyl)pyridinium salt. The yield of *N*-(pentamethylbenzyl)acetamide was determined by gas chromatography relative to 1,3,5-tri-*tert*-butylbenzene as the internal standard. The conversion of durene to (2,4,5-trimethylbenzyl)lutidinium salt (δ 5.5) was measured with nitromethane (δ 4.3) as the internal standard for NMR analysis. GC-MS analysis also indicated the presence of *N*-(trimethylbenzyl)acetamide by its cracking pattern, but it was not otherwise identified. However, a careful search was made for the presence of 2,3,5,6-tetramethylacetanilide (corresponding to the product of nuclear substitution by acetonitrile) by comparison of the gas chromatographic behavior of an authentic sample (vide supra). None was detected.

All the results of the product analysis for oxidations in acetonitrile are summarized in Table VI.

A solution of hexamethylbenzene (0.0113 mmol) and Fe(phen)₃(PF₆)₃ (0.0124 mmol) in 5 mL of trifluoroacetic acid was sealed in a glass vial under argon. The vial was heated on a steam bath for approx 10 min or until the iron(III) complex was completely dissolved. After standing for 2 h at room temperature to ensure completion, the reaction mixture was concentrated under a stream of argon, and 2 mL of CH₂Cl₂ were added together with a weighed amount of tri-*tert*-butylbenzene as the internal standard. The mixture was extracted with water and the CH₂Cl₂ layer analyzed by gas chromatography. The yield of pentamethylbenzyl trifluoroacetate⁶⁵ was 96% based on the recovered hexamethylbenzene and 76% based on the iron(III) consumed in a 2:1 stoichiometry.

Kinetic Measurements. Solutions of 0.05–2 mM iron(III) in acetonitrile were examined spectrophotometrically whenever possible under

(59) Gonzales, A. G.; Aguiar, J. M.; Martin, J. D.; Rodriguez, M. L. *Tetrahedron Lett.* 1976, 205.

(60) Photochemical chlorination of hexamethylbenzene (Chen, K. S.).

(61) Smith, J. W. *J. Chem. Soc.* 1961, 4700.

(62) Smith, L. I.; Moyle, C. L. *J. Am. Chem. Soc.* 1933, 55, 1676.

(63) Smith, L. I.; Tenenbaum, D. *J. Am. Chem. Soc.* 1935, 57, 1293.

(64) Birtles, R. H.; Hampson, G. C. *J. Chem. Soc.* 1937, 10.

(65) Lau, W.; Huffman, J. C.; Kochi, J. K. *J. Am. Chem. Soc.* 1982, 104, 5515.

Table VI. Product Analysis from Methylarenes and Tris(phenanthroline)iron(III) in the Presence of Bases^a

methylarene	mmol	MeCN, mL	FeL ₃ ³⁺ , mmol	base, ^b mmol	ArCH ₃ B ⁺ , % ^c
C ₆ (CH ₃) ₆	0.06	2	0.10	lu (0.43)	60
C ₆ (CH ₃) ₆	0.53	20	1.0	py (0.99)	78 ^d
C ₆ H ₂ (CH ₃) ₄ -1,2,4,5	5.7	4	0.2	lu (2.6)	75 ^e
C ₆ H ₄ (CH ₃)(OCH ₃)-1,2	2.4	2	0.1	lu (4.3)	80

^a In acetonitrile at 25 °C. ^b lu = 2,6-lutidine, py = pyridine. ^c Yield based on complete disappearance of two iron(III) for each arene.

^d Based on 90% conversion of iron(III); *N*-(pentamethylbenzyl)acetamide (11%) found. ^e *N*-(2,4,6-Trimethylbenzyl)acetamide also detected.

Table VII. Contribution from Diffusion to the Rate Constant for Electron Transfer

(5-X(phen)) ₃ Fe ³⁺	rate constant ^a	methylarene			
		HMB	PMB	DUR	TMB
H	{ k ₁ k ₂	14	0.28	3.0 × 10 ⁻²	5.1 × 10 ⁻³
		14.5	0.32	4.2 × 10 ⁻²	5.3 × 10 ⁻³
Cl	{ k ₁ k ₂	52	5.3	3.8	2.8
		52	5.6	14.6	4.6
NO ₂	{ k ₁ k ₂	1.3 × 10 ³	75	16	4.1
		1.3 × 10 ³	76	17	4.2

^a Rate constants in M⁻¹ s⁻¹.

pseudo-first-order conditions with >10-fold excess methylarene (0.4–200 mM) and varying amounts of base (pyridine or lutidine, 4–500 mM) in a 1.0-cm quartz cuvette, preflushed with argon. (The same results were obtained when Schlenk techniques were used to remove air.) The absorbance of either the iron(II) complex at 510 nm (for solutions containing <0.3 mM [Fe(III)]₀) or the iron(III) complex at 650 nm (for solutions containing >1 mM [Fe(III)]₀) was monitored at intervals ranging from 1 to 5 s with the aid of a diode array spectrophotometer (vide supra) at 22 °C.

The kinetics were generally followed to beyond 99% conversion. The absorbance *A* was related to the extent of reaction as [Fe(III)]/[Fe(III)]₀ = (A_t - A_∞)/(A₀ - A_∞). The rate constants *k*_{obsd} for reactions carried out under pseudo-first-order conditions were obtained for a plot of ln [Fe(III)]/[Fe(III)]₀ against the time *t*. Figure 13 shows that the slope of such a graph is calculated to be linear from -ln[Fe(III)]/[Fe(III)]₀ = 1.0 to 5.0 to a precision greater than 99%. Indeed we found the rate data from -ln[Fe(III)]/[Fe(III)]₀ = 1.4–4.6 (corresponding to >99% conversion) to be essentially linear, although the slope was usually measured to 2.3. A factor of 2 was included in the slope to take into account the stoichiometry. For experiments run under second-order conditions, i.e., [Fe(III)]₀ = [ArCH₃]₀/2, the value of ([Fe(III)]₀/[Fe(III)] - 1) was plotted against the time, and the slopes were measured from 0 to 5.0.

Control runs in the absence of methylarenes were required to assess quantitatively the consumption of iron(III) by the added base. The competition from the base B was assumed to have the form

$$k_{\text{obsd}} = k_{\text{B}}[\text{B}] + k_{\text{e}}'[\text{ArCH}_3] \quad (29)$$

For example, in an experiment utilizing 3.7 mM HMB, 0.07 mM Fe(phen)₃³⁺, and 530 mM py in acetonitrile containing 0.1 M TEAP, the value of *k*_{obsd} was 0.134 s⁻¹. The same system in the absence of HMB afforded *k*_{obsd} = *k*_B[B] = 0.049 s⁻¹. Accordingly from eq 29, we obtain *k*_e' = (0.134 - 0.049)/[ArCH₃]₀ = 22 M⁻¹ s⁻¹. At py concentrations less than 100 mM, the contribution from *k*_B was negligible, and thus *k*_{obsd} = *k*_e'[ArCH₃]₀. By this procedure, the competing contribution from the base was evaluated independently with every system examined. It also afforded optimal values of the ratio [B]/[Fe(III)]₀ for the determination of *k*₁ in eq 15. The kinetic results in Table III for the 5-chloro- and 5-nitrophenanthroline complexes were obtained at a single base concentration corresponding to this optimal ratio.

Electrochemical Measurements. The electrochemical determinations of the standard oxidation potentials for the tris(phenanthroline)iron(II) complexes and their derivatives were performed by cyclic voltammetry in acetonitrile containing 0.1 M TEAP. The CV waves were totally reversible (*i*_p^c/*i*_p^a = 1.0) for all the scan rates investigated (0.1–0.5 V s⁻¹). The working electrode consisted of a platinum disc of 1-mm diameter imbedded in a cobalt glass seal. It was polished with a 30-μm silicon carbide abrasive and rinsed with water and acetone before use. The counter electrode was a platinum mesh of ~1 cm² area. The reference electrode was a standard calomel electrode separated from the anolyte by a 0.1 M TBAP solution of acetonitrile. The potentiostat was a Princeton Applied Research Model 173 equipped with a Model 176 current/voltage converter for ohmic drop compensation and with a high-impedance voltage amplifier (Model 178). The input potential was provided by a PAR Model 175 universal programmer, and the output was recorded on a Houston series 2000 x-y recorder.

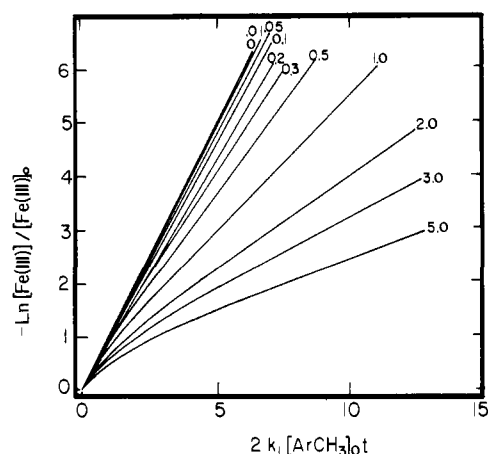


Figure 13. First-order kinetic dependence of iron(III) disappearance under pseudo-first-order conditions, as calculated according to eq 10. The numbers associated with the curves are the values of *k*₁[Fe(III)]₀/(*k*₃ - [py]). Compare with Figure 2.

The 5-chloro- and 5-nitrophenanthroline derivatives of Fe(phen)₃³⁺ were prepared by constant-potential (*E* = *E*⁰ + 0.1 V) electrolysis of the corresponding iron(II) complex in a 10-mL air-tight cell under an argon atmosphere. The working electrode was a platinum gauze of ~2-cm² area. The counter electrode was a chromel wire of ~3-cm² area, which was separated from the anolyte with a glass frit. A charge of 1 *F* was passed for each mole of iron(II), and the electrolyzed solution was stored under argon until spectral analysis and use.

The cyclic voltammograms of ArCH₃ by and large showed irreversible chemical behavior at scan rates *v* < 200 V s⁻¹ in acetonitrile solutions. However, reproducible, reversible cyclic voltammograms of hexamethylbenzene, pentamethylbenzene, and durene were obtained at a platinum electrode with *v* = 200 V s⁻¹ in trifluoroacetic acid containing 5 vol % trifluoroacetic anhydride and 0.1 M tetrabutylammonium perchlorate. The values of *E*⁰ and 1/2(*E*_p^a + *E*_p^c) reported in Table I are applicable to studies in acetonitrile since there exists a linear correlation between *E*⁰ obtained in this manner for these polymethylbenzenes and the gas-phase ionization potential *I*_p, [viz., *E*⁰ (V vs. SCE) = 1.00*I*_p (eV) - 6.35].⁶⁶ Thus the contributions from solvation on *E*⁰ are rather invariant, and only a constant difference need be considered for *E*⁰ of various arenes from one solvent to another. [For use in the free energy relationships, the difference was considered to be 0.12 V, i.e., *E*_{Ar}⁰(ACN) = *E*_{Ar}⁰(TFA) - 0.12 V]. The *E*⁰ for prehnitene was estimated from the correlation of *E*_p (the anodic peak potential in CH₃CN at 0.1 V s⁻¹) and *E*⁰ (trifluoroacetic acid/anhydride previously established for 15 alkylbenzenes).⁶⁷ The values of *E*_p and *E*⁰ for hexamethylbenzene and

(66) Amatore, C., unpublished results. Compare with: Dewar, M. J. S.; Hashmall, J. A.; Trinajstić, N. *J. Am. Chem. Soc.* 1970, 92, 5555.

(67) Howell, J. O.; Goncalves, J.; Amatore, C.; Klasinc, L.; Wightman, R. M.; Kochi, J. K. *J. Am. Chem. Soc.*, in press.

hexamethylbenzene- d_{18} were the same to within the experimental uncertainties.

Electron Spin Resonance Studies of Arene Cation Radicals as Intermediates. The direct observation of arene cation radicals as intermediates in the oxidative substitutions with iron(III) was carried out as follows. Separate trifluoroacetic acid solutions of 6.3 mM hexamethylbenzene and $\text{Fe}(\text{phen})_3(\text{PF}_6)_3$ (prepared from 11 mg of complex and 2.0 mL of solvent by heating over a steam bath until complete dissolution) were added to an ESR tube with a side arm affixed. The tube was sealed in vacuo, and the contents were mixed by rapid shaking immediately prior to insertion in the ESR cavity (Varian E-112). The concentration of $\text{HMB}^{\cdot+}$ was followed periodically by monitoring the intensity of the $M_1 = 0$ line. The dashed line in Figure 1 indicates that 15–20 s were required to obtain the first data point. Since the disappearance of the cation radical was temperature dependent, the ESR spectrum shown in the inset was obtained from a similar reaction which was cooled to -30°C prior to mixing.

Evaluation of the Free Energy Terms. The free energy change $\Delta G_o'$ was determined from the standard oxidation potentials in Table I according to eq 20. The work term w_p was considered to be only of electrostatic origin, i.e., $w_p = 2e^2/Dd^*$ as given in ref 45. The activation free energy ΔG^\ddagger was evaluated from the rate constant k^* listed in Table III and eq 21, where $w_r \cong 0$ and the collision frequency was taken to be $10^{11} \text{ M}^{-1} \text{ s}^{-1}$. The value of k^* was deduced from k_1 by taking into account the diffusional contributions according to eq 17.³⁶ For rapid oxidative substitutions, the effect of diffusion on k_1 is small, but increases in importance for the slowest rates, as shown in Table VII.

The intrinsic barriers were computed from the values of $\Delta G_o'$ and ΔG^\ddagger for each system, with the aid of the free energy relationship in eq 22–24. For each methylarene, the three values of ΔG_o^\ddagger (obtained with the three iron(III) oxidants) were averaged for construction of Figure 6.

Derivation of the Kinetic Rate Expressions. The kinetics were based on the stoichiometry in eq 6 and the mechanism presented in Scheme II for the general case in which back electron transfer (k_{-1}) competes with the followup step (k_3). All derivatives assumed a zero order dependence on arene (Ar) in excess, and a negligible consumption of the pyridine base. The rate of iron(III) disappearance (taking into account the steady state concentration of $\text{ArCH}_2^{\cdot+}$) is

$$-d[\text{Fe}(\text{III})]/dt = k_1[\text{Fe}(\text{III})][\text{Ar}] - k_{-1}[\text{Fe}(\text{II})][\text{Ar}^{\cdot+}] \quad (30)$$

Since at steady state, $[\text{Ar}^{\cdot+}] = k_1[\text{Fe}(\text{III})][\text{Ar}]/(k_{-1}[\text{Fe}(\text{II})] + k_3[\text{py}])$, eq 30 reduces to

$$-d[\text{Fe}(\text{III})]/dt = 2k_1[\text{Fe}(\text{III})][\text{Ar}]\{1 - k_{-1}[\text{Fe}(\text{II})]/k_{-1}[\text{Fe}(\text{II})] + k_3[\text{py}]\} \quad (31)$$

For $[\text{Fe}(\text{II})] = [\text{Fe}(\text{III})]_0 - [\text{Fe}(\text{III})]$ and $x = [\text{Fe}(\text{III})]/[\text{Fe}(\text{III})]_0$, eq 31 is simplified to

$$(-dx/x)(1 - x + k_2[\text{py}]/(k_{-1}[\text{Fe}(\text{III})]_0)) = (2k_1[\text{Ar}]k_3[\text{py}]/(k_{-1}[\text{Fe}(\text{III})]_0)) dt \quad (32)$$

Integration of eq 32 between the limits of $t = 0$ ($x = 1$) and $t(x)$ yields

$$(1 + p)\ln x + p(1 - x) = -2k_1[\text{Ar}]t \quad (33)$$

where $p = k_{-1}[\text{Fe}(\text{III})]_0/(k_3[\text{py}])$.

Two limiting situations derive from eq 33, that is, $p \cong 0$ and $p \gg 1$, which describe rate-limiting electron transfer (eq 14) and pre-equilibrium electron transfer (eq 12), respectively. The same results are obtained in the latter case, if $[\text{Ar}^{\cdot+}]$ is assumed to attain equilibrium rapidly, i.e., $k_1/k_{-1} = [\text{Ar}^{\cdot+}][\text{Fe}(\text{II})]/([\text{Fe}(\text{III})][\text{Ar}])$.

Note that the previously measured rate constants^{12e} did not take into account the reversibility in the electron transfer. Correction of this factor, however, does not fundamentally affect the conclusions presented therein.

Acknowledgment. We thank the National Science Foundation for financial support of this research and for a fellowship to C.A. under the auspices of the United States–France (NSF-CNRS) cooperative program, Dr. W. Lau for help with the ESR experiments, and J. Goncalves for the computer interface of the spectral data.

Registry No. $(\text{phen})_3\text{Fe}^{2+}$, 14708-99-7; $(5\text{-Cl}(\text{phen}))_3\text{Fe}^{2+}$, 15053-59-5; $(5\text{-NO}_2(\text{phen}))_3\text{Fe}^{2+}$, 15245-50-8; $(\text{phen})_3\text{Fe}^{3+}(\text{PF}_6)_3^-$, 28277-57-8; $(5\text{-Cl}(\text{phen}))_3\text{Fe}^{3+}(\text{PF}_6)_3^-$, 89556-59-2; $(5\text{-NO}_2(\text{phen}))_3\text{Fe}^{3+}(\text{PF}_6)_3^-$, 89578-85-8; $\text{C}_6\text{H}_4(\text{CH}_3)(\text{OCH}_3)\text{-1,2}$, 578-58-5; HMB, 87-85-4; HMB- d_{18} , 4342-40-9; PMB, 700-12-9; DUR, 95-93-2; TMB, 488-23-3; *p*-methoxytoluene, 104-93-8; pyridine, 110-86-1; deuterium, 7782-39-0.

Stereochemical Course of the Autoxidative Cyclization of Lipid Hydroperoxides to Prostaglandin-like Bicyclo Endoperoxides

D. E. O'Connor,* E. D. Mihelich,[†] and M. C. Coleman

Contribution from The Procter & Gamble Company, Miami Valley Laboratories, Cincinnati, Ohio 45247. Received September 26, 1983

Abstract: The stereochemical course of the autoxidative cyclization of the two polyunsaturated fatty acid hydroperoxides **1a** and **1b** to form prostaglandin-like bicyclo endoperoxides has been found to be highly selective. The reaction generates four independent chiral centers, giving rise to the possibility of eight different stereoisomers having the basic prostaglandin structure. Seven of these eight diastereoisomers were observed: four, representing three different ring stereochemistries, were isolated and characterized as relatively pure single isomers; three others were characterized as minor components of the major isomers. The major bicyclo endoperoxide products of the reaction were the two C-15 epimers of the endo,endo bicyclo endoperoxides **9** and **10**. While the two C-15 epimers of the exo,exo bicyclo endoperoxides **7** and **8** were also formed in significant yield, the products arising from trans ring substituents (including those having the natural prostaglandin ring stereochemistry) were only minor components. Interestingly, the isomers that could arise from oxygenation of intermediate **6** at the carbon adjacent to the bicyclic ring were not observed. Thus, the reaction shows high selectivity disfavoring the formation of the natural prostaglandin stereochemistry.

Since their discovery by von Euler, Goldblatt, and Kurzkrook,¹ the prostaglandins have been noted for their remarkably potent and varied biological effects. It was not until the early 1960s that the complete structures were elucidated for "primary" prostaglandins (PGF's, PGE's), and in the ensuing two decades the astounding complexity of the arachidonic acid cascade has slowly become apparent.² The common intermediate to all the pros-

taglandins, thromboxanes, and prostacyclin is the bicyclo endoperoxide PGG, which results from the action of the prostaglandin synthetase (cyclooxygenase) enzyme on 20-carbon polyunsaturated

(1) A concise historical perspective is given by: von Euler, U. S. In "Progress in Lipid Research"; Holman, R. T., Ed.; Pergamon Press: Elmsford, NY, 1982; Vol. 20, pp xxxi–xxxv.

(2) Nelson, N. A.; Kelly, R. C.; Johnson, R. A. *Chem. Eng. News* 1982, 60 (33), 30–44.

[†] Present address: Eli Lilly & Co., Indianapolis, IN 46285.